Inhibition of *C. zeina* Cdc14 can have broad applications in fungicide development

Gbenoba, J. Gong, E. Kang, D.

ABSTRACT

***Cercospora zeina* is a fungal pathogen that causes grey leaf spot (GLS), a disease that harms maize crops (1). Recent research indicates that Cercospora species are developing resistance to current generic fungicides, making it necessary to develop new means of fungal inhibition (2). While *C. zeina* is not a well-studied species, the *CDC14* gene serves as a potential solution to the issue of GLS; it has been shown that deletion of this gene, which is highly conserved across the fungal kingdom, reduces the ability of fungal pathogens similar to *C. zeina* to infect their host plants (2). In the interest of fungicide development, the CzCdc14 protein was purified and its enzymatic properties characterized prior to the testing of small-molecule inhibitor candidates. The best-performing inhibitor molecule during in vitro experimentation was I1 (refer to Supplemental Figure 7), which was also one of the inhibitors predicted to be most effective in the Molecular Operating Environment (MOE) software. The potential viability of the I1 molecule as a CzCdc14 inhibitor, taken together with the aforementioned conservation of the fungal Cdc14 active site, has important implications for controlling the spread of not only GLS, but other fungal crop diseases as well.**

INTRODUCTION:

The fungal species *Cercospora zeina* has been identified as a cause of major crop failures in Asia, the Americas, and Africa (3). It is in these regions that *C. zeina* infects maize with grey leaf spot (GLS), a disease that allows *C. zeina* to necrotrophically attack its host plants with the mycotoxic chemical cercosporin (1, 4, 5). The spread of GLS is most effective in warm and humid conditions, and occurs by spore dispersal and the planting of crops in soil where infected residues remain (5).

Maize is one of the most important crops in the agricultural industry, with almost 717 million metric tons harvested each year (6). GLS can thus have massive economic and agricultural consequences: the disease typically lowers crop yield by 25% for infected fields, but losses of up to 100% are not uncommon (7, 8). Further, efforts to combat GLS have seen limited success. One method has been the application of foliar pesticides such as QoI (quinone outside inhibitor) fungicides in the United States and South Africa (9). However chemical treatments result in a selective pressure for fungicide resistance in *Cercospora* species, necessitating the continuous development of new methods to addressing GLS outbreaks (9).

Encouragingly, however, the cell division control gene *CDC14* may be able to serve as a fungicide target in *C. zeina*. *CDC14* is highly conserved within the fungal Kingdom. *Fusarium graminearum*, *Magnaporthe oryzae*, and *Aspergillus flavus* were shown to lose their ability to attack their target plants when they lacked this gene (2). In yeast, *CDC14* encodes a phosphatase involved in regulation of the fungal cell cycle and reproduction process (10, 11). In *Saccharomyces cerevisiae*, Cdc14 helps bring about autophagy, a process of lysosomal degradation necessary for meiotic entrance and exit (2). In *Schizosaccharomyces pombe*, Cdc14 assists in mitotic exit by inhibiting the Clb kinase, whose activity causes cells to remain the S or mitosis phases of the cell cycle (11). A fungicide that inhibits Cdc14 may thus prevent the spread of GLS by impeding cell division in *C. zeina*.

Cdc14 has been classified as a dual-specificity phosphatase, a type of protein-tyrosine phosphatase capable of dephosphorylating substrates at Ser/Thr or Tyr residues (12). Extensive research has already been conducted regarding this and other features of Cdc14 substrate binding and it has been shown that the protein tends to adhere to a general set of recognition requirements across fungal species. Given that such features appear across multiple fungal species, a selected inhibitor can be used against fungal pathogens beyond *C. zeina*.

It is predicted that a Cdc14-targeting fungicide will harm neither treated maize nor the organisms that consume it. Though the catalytic residues of Cdc14 are highly conserved and likely to be present in both fungi and humans, the function of the Cdc14 protein is not so highly conserved between these lineages; animal mitotic exit apparently depends not on Cdc14, but on PP1 and PP2A phosphatases (10). Furthermore, it has been found that *CDC14* was absent in the common ancestor of angiosperms, and analysis of model plant genomes has revealed that the *CDC14* gene may not be present within many land plants (2).

The high degree of conservation of the CzCdc14 active site residues suggests that Cdc14 plays the same essential role in the life cycle and reproduction of *C. zeina* as it does in similar organisms. It may thus be possible to develop a pesticide that can be used to prevent not only GLS, but other fungal crop diseases as well. In this study, the function of CzCdc14 was characterized by determination of various kinetic parameters such as K_{cat}, K_M and the IC_{50} of inhibitor candidates discovered through high-throughput screening.

PROCEDURE:

Three-dimensional structure prediction and analysis.

Homology model development.

The amino acid sequence of CzCdc14 was input as a query sequence into the Molecular Operating Environment (MOE, Chemical Computing Group) software, yielding the crystal structure of *Saccharomyces cerevisiae* Cdc14 (ScCdc14) as the top hit. The ScCdc14 sequence (5XW5, with the Swi6 phosphopeptide ligand bound) was used as the basis for the generation of the homology model for CzCdc14.

Determination of active site residues.

Because site-directed mutagenesis had been done on the 5XW5 sequence to change a catalytic Cys to a Ser residue, this active-site Ser was manually reverted to Cys to match the wild-type sequence of ScCdc14. The CzCdc14 homology model was then aligned with 5XW5, allowing for selection of pocket residues. Ligand interaction maps were generated to compare the interactions of Swi6 with the 5XW5 active site to Swi6 interactions with the homology model active site.

Conservation of specificity analysis.

The amino acid sequence of CzCdc14 along with the amino acid sequences of related fungal species (*Alternaria alternata*, *Penicillium digitatum*, *Puccinia coronata*, *Rhynchosporium commune*, *Ustilago hordei*) were input into Clustal Omega to generate a multiple sequence alignment. Residues within and immediately outside of the binding pocket were compared to find sequence differences that could have resulted from evolutionary divergences.

Protein Expression and purification

Expression

E. coli BL21 AI cells were transformed via standard procedure with a pET-15b plasmid containing the A sub chain of *CDC14* from *C. Zeina* (2). A 100x cell dilution and the original cell culture were transferred to agar plates containing ampicillin and incubated at 37 ^{o}C for 16 hours.

Cells from a single colony were transferred into three tubes of 2xYT medium and incubated at 37 ^{o}C and 225 rpm in a rotary incubator for 16 hours. 500mL of solution were placed into each of two sterile Fernbach flasks containing 2xYT growth medium and ampicillin. The flasks were then incubated at 22 ^{o}C and 225 rpm for 9 hours. After the optical density of the solution exceeded 0.7 at a wavelength of 600 nm, a 1 mL sample of uninduced cells was extracted and stored. L-arabinose was added to the Fernbach flasks to a final concentration of 0.1% to induce expression of CzCdc14. The induced cell cultures were incubated at 22 ^{o}C and 225 rpm for another 16 hours.

A 1 mL sample of induced cells was taken from the Fernbach flasks and the remaining induced cells were pelleted by centrifugation at 4 ^{o}C and 3500 rpm for 20 minutes. The supernatant was discarded and the cell pellet was stored at -80 ^{o}C. 2x SDS gel-loading buffer, dithiothreitol (DTT), and ddH_2O were added to the 1 mL samples of induced and uninduced cells, which were then incubated at 95 ^{o}C for 5 minutes and stored at -20 ^{o}C.

The cell pellet was resuspended in a solution of lysis buffer (25 mM HEPES [pH 7.5], 500 mM NaCl, 0.1% [v/v] Triton x-100, 10 mM imidazole, 10% [v/v] glycerol), 1 mg/mL lysozyme, 10 µM leupeptin, 1 µM pepstatin, and universal nuclease and incubated on ice for 30 minutes before the addition of phenylmethylsulfonyl fluoride to a final concentration of 0.5 mM. After cell lysis, the cellular debris were removed via centrifugation at 4 ^{o}C for 30 minutes at 15000*g*. The supernatant was transferred into a pre-chilled conical tube. Then, 15 µL of this solution was added to 2x SDS-gel loading buffer and 1 M DTT, incubated at 95 ^{o}C for 5 minutes, and then stored at -20 ^{o}C.

Purification

Nickel Buffer A (25 mM HEPES [pH 7.5], 500 mM NaCl, 0.1% [v/v] Triton x-100, 10% [v/v] glycerol) was used to wash the chromatography column apparatus. Next, a solution containing Ni-NTA beads was transferred into the chromatography column. Nickel Buffer A was used to wash the Ni-NTA beads. Different concentrations of imidazole (40 mM, 100 mM, 250 mM) were produced by combining varying proportions of Nickel Buffer A and Nickel Buffer B (25 mM pH 7.5 HEPES, 500 mM NaCl, 250 mM imidazole, 10% [v/v] glycerol). These imidazole solutions were then run through the column. Afterwards, Milli-Q® water and ethanol were run through the column. The flow through rate was held at roughly 1 mL/min and each run-through solution was stored at -4 ^{o}C.

The 100 mM imidazole wash solution was transferred to dialysis tubing, submerged in 1 L of storage buffer and stirred at -4 ^{o}C overnight. The contents of the tubing were separated into 250 µL aliquots and stored at -80 ^{o}C.

SDS-PAGE

Molecular weight markers, uninduced cells, induced cells, cell lysate solution, flow-through 2 (cell lysate twice-passed through nickel column), Buffer A wash, 40 mM imidazole wash, 100 mM imidazole elution, and 250 mM imidazole regeneration were prepared and incubated at 95 ^{o}C for 5 minutes. 5 µL of MW markers and 30 µL of each of the samples were placed into the polyacrylamide gel and 1x Tris-Glycine SDS (TGS) buffer before being run through a voltage gradient of 200 V for approximately 1 hour. The gel was stained with Coomassie Blue and de-stained in an acetic acid solution. A digital image of the gel was produced via the Bio-Rad Gel Doc EZ imaging system.

Bradford assay.

A standard curve was generated with bovine serum albumin (BSA) standards from 50 to 800 ug/mL. These were treated with Bradford dye reagent and vortexed, and absorbance values were taken at 595 nm. 10x and 25x dilutions of previously purified CzCdc14 were created. Three absorbance measurement trials were conducted for each of these CzCdc14 concentrations at 595 nm. These measurements and the standard curve equation were used to calculate protein concentration.

Nanodrop spectrophotometry.

A nanodrop spectrophotometer was used to analyze the 25x target protein dilution. The extinction coefficient for CzCdc14 (69,790 M^{-1} cm^{-1} under the assumption that all cysteines are reduced) was obtained from the Expasy program in order to calculate a protein concentration independent of that obtained from the aforementioned Bradford assay.

Activity assay.

A pNP standard curve was generated using concentrations ranging from 0.5 to 100 µM with 25mM diethylamine (DEA) as a diluent. Next, a continuous linearity assay was run at various enzyme concentrations to determine the linear range and optimal protein concentration for future assays. An inhibition assay was then run in triplicate in a 96-well microplate where one set of trials included sodium tungstate at a final concentration of 2 mM in place of an equivalent volume of reaction buffer. Enzyme was added to start the reaction and 5 N NaOH to end the reaction. Absorbance values were measured at 405 nm, converted into [pNP] using the standard curve, and used to calculate specific activity for CzCdc14 with and without the sodium tungstate inhibitor.

Steady-state assay.

Reaction wells containing varying concentrations of para-Nitrophenyl phosphate (2 mM to 80 mM pNPP) as a substrate, CzCdc14 enzyme (at a concentration chosen based off the results from a previously-conducted linearity assay), 1M DTT, and enzyme reaction buffer (25 mM HEPES, 1 mM EDTA, 150 mM NaCl). Blank wells contained the same components save CzCdc14, which was replaced by an equivalent volume of enzyme reaction buffer. Enzymatic activity was stopped by the addition of 5 N NaOH. The absorbance values of the well solutions were measured at 405 nm and converted into [pNP] values using the aforementioned standard curve. These concentration values were used to calculate initial velocities, which in turn were used to generate a steady state kinetic analysis curve based on the Michaelis-Menten equation:

$$V_0 = \frac{V_{max} \times [S]}{K_m + [S]}$$

Phosphopeptide substrate assay.

To generate a standard curve, varying sodium phosphate concentrations (ranging from 2.5 uM to 30 uM) and enzyme reaction buffer were added into a 96-well plate along with a fixed volume of Biomol Green. After incubation for approximately 20 minutes at room temperature, the plate was scanned at 640 nm. Next, constant volumes and concentrations of a variety of phosphopeptide substrates, 1M DTT, enzyme reaction buffer, CzCdc14, and ddH_2O were added to a new microplate. The reactions were started by adding CzCdc14, run for 20 minutes and stopped with Biomol Green. The plates were left to incubate for approximately 20 minutes and then scanned with a microplate reader at 640 nm. The data was used to determine binding affinity for different substrates by calculating their specificity constants.

Inhibition assay.

A Z-factor was calculated via the equation below to determine the ideal conditions for a CzCdc14 inhibition assay.

$$Z - factor = 1 - \frac{3 \times (\sigma_p + \sigma_n)}{|\mu_p - \mu_n|}$$

P represents trials with no inhibitors to simulate 100% enzyme activity, and N represents trials with no enzyme to simulate 100% inhibition. Z-factor determination involved conducting two sets of 3 trials: the first set contained CzCdc14 and the second did not (CzCdc14 was replaced by enzyme reaction buffer). In all 6 trials, the same volumes and concentrations of substrate, 1M DTT, and NaOH (to stop enzymatic activity) were used. In the subsequent inhibition assay, the two most effective inhibitors were used in three trials containing pNPP substrate, reaction buffer, enzyme, inhibitor, and NaOH (added to stop enzymatic activity). The blanks contained the same components as the experimental wells, apart from enzyme, which was replaced by enzyme reaction buffer. The well plates were scanned by the plate reader at 405 nM. The data was used to determine the IC_{50} of the selected inhibitors.

RESULTS:

3.1 Confirmation of Cdc14 in C. zeina

After bacterial transformation of *E. coli,* experiments were conducted to isolate CzCdc14 from the cell lysate solution. Nickel-column chromatography was used to extract pure protein using

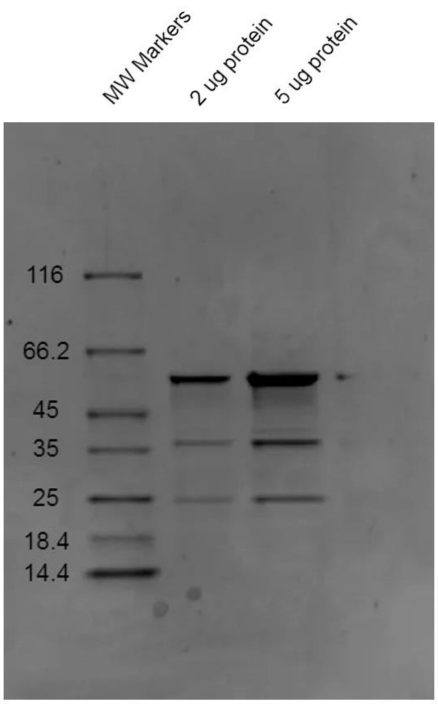

Figure 1. SDS-PAGE following protein purification by nickel affinity chromatography. Purified *C. zeina* Cdc14 was analyzed on a standard-issue acrylamide gel run with 200 volts for one hour in a tris-glycine-SDS buffer solution. From lane 1 to lane 3: molecular weight markers, 2 μg of protein, and 5 μg of protein. The ImageLab software (used for gel image analysis) provides an estimated molecular weight of 55.1 kDa based off the darkest band in the 5 μg lane, which is comparable to the predicted molecular weight of 58.21896 kDa obtained from the Expasy program.

imidazole washes and these solutions were stored for future testing. The imidazole wash solutions were used for SDS-PAGE gel testing as presented below.

As shown in Figure 1, bands from the SDS-PAGE indicated presence of proteins in imidazole washes, which were most likely CzCdc14 after bacterial expression of the enzyme. Using the darkest band that indicated the highest concentration of preserved CzCdc14, molecular weight of the enzyme was determined to be roughly 55.1 kDa. A calculation independent of the SDS-PAGE gel was made to confirm the molecular weight of CzCdc14 via Expasy molecular weight software. Inputting the amino acid sequence into the Expasy software gave a final molecular weight result of roughly 58.21896 kDa, in excellent agreement with the experimentally determined molecular weight.

3.2 Determination of concentration of Cdc14 within solution

Following nickel column purification, the protein aliquots collected were analyzed by two methods. A Bradford assay was first conducted to determine protein concentration based off of spectrophotometric readings. A BSA curve (shown in Suppl. Figure 1) was used to convert absorbance values to concentrations (uM), resulting in a CzCdc14 concentration estimate of 126 μM.

The second method used to determine protein concentration was nanodrop spectrophotometry. The extinction coefficient for the CzCdc14 sequence (with His-tag attached) was given as 69,790 M^{-1} cm^{-1} (assuming reduction of all cysteines) by the Expasy software. This value was used with the nanodrop concentration reading (0.345 mg/mL) to yield a concentration estimate of 123.58 μM, in exceptional agreement with the Bradford assay. The average of these estimates – 124 $\pm$ 3 μM – was used for all future calculations where appropriate.

3.3 Activity Assays

To determine the activity of the purified CzCdc14 enzyme, a pNPP linearity assay was run for the purpose of observing the rate of product (para-Nitrophenyl) formation at different enzyme concentrations. The results of this assay allowed for the determination of the parameters within which CzCdc14 operates under steady-state conditions.

As shown in Figure 2, enzyme concentrations of 100 nM and 300 nM exhibited a linear change in absorbance for an extended period of time, indicating a constant rate of product formation. The absorbance was compared to the standard curve to determine the conditions under which CzCdc14 would adhere to the steady-state assumption. These parameters were then used in all future pNPP assays.

After the standard curve for pNP had been generated (shown in Suppl. Figure 2), an assay was run in which some reaction wells contained sodium tungstate–a common inhibitor of Cdc14 phosphatases (13)–was present in some reaction wells and absent in others.

Additionally, research characterizes sodium tungstate as a potent inhibitor of all phosphatase activity (13). As shown in Figure 11, resulting data indicated that there was enzymatic activity in assays run in the absence of sodium tungstate as seen in the higher specific activity, reinforcing the hypothesis that CzCdc14 is a phosphatase. Moreover, the enzymatic activity for the wells that were run in the presence of sodium tungstate were significantly lower than the absorbance value results from the wells run without the presence of sodium tungstate, again indicating that CzCdc14 is a phosphatase as sodium tungstate is a known inhibitor for Cdc14 phosphatases. To further verify this claim, the average specific activity (pmol product/min/pmol enzyme) of CzCdc14 was calculated for both uninhibited and inhibited trials. Trials conducted in the absence of sodium tungstate (no

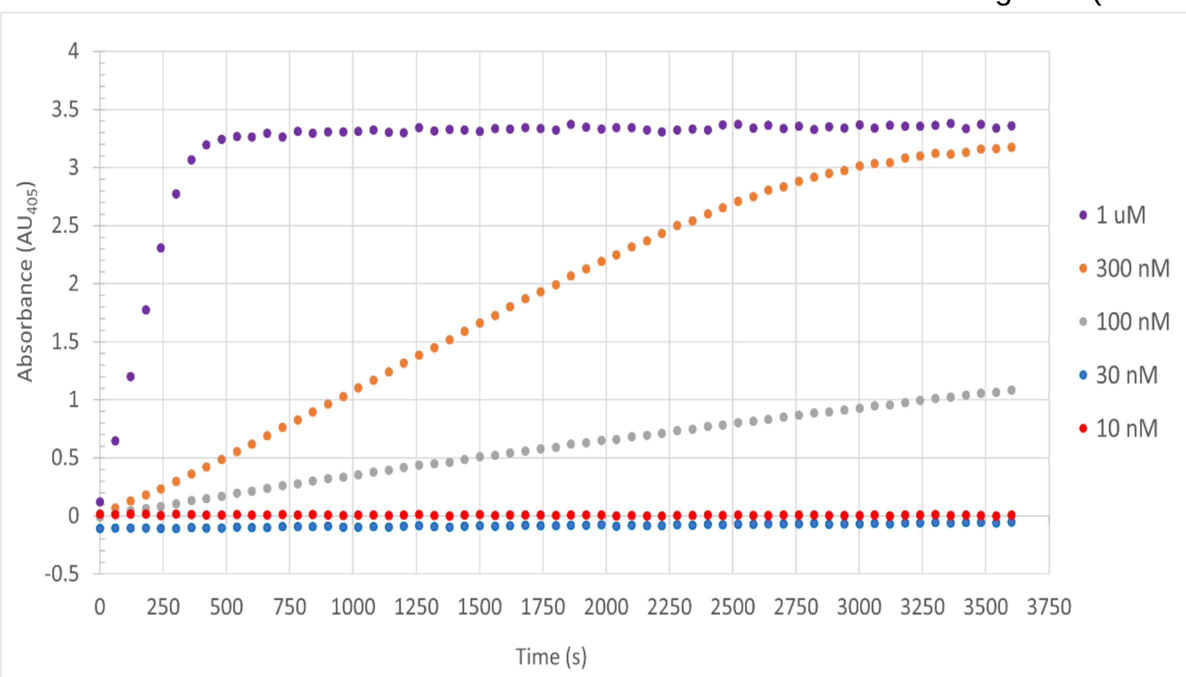

Figure 2. Continuous *para*-Nitrophenyl phosphate (pNPP) assay at differing concentrations of CzCdc14. Enzyme concentrations ranging from 10 nM to 1 uM are run in the continuous assay with 40 mM pNPP for 60 minutes, with the plate reader taking absorbance measurements at 405 nm once every minute.

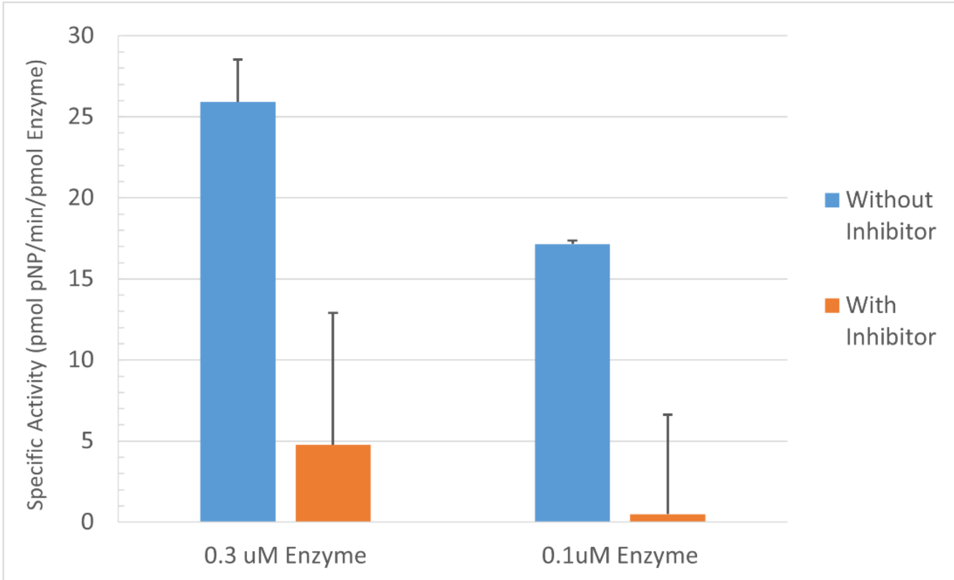

Figure 3. CzCdc14 activity in response to the presence or absence of sodium tungstate. Six trials of each protein concentration are conducted; three inhibited and three uninhibited by sodium tungstate. The phosphatase inhibitor sodium tungstate is added to a 2 mM concentration in inhibited reactions. The average and standard deviation of the three trials for each condition are represented as the bars and error bars respectively.

inhibitor) had an average of 25 $\pm$ 3 and 17.1$\pm$ 0.2 pmol product/min/pmol enzyme for 0.3uM and 0.1uM enzyme concentrations respectively, whereas trials with the presence of sodium tungstate had an average of 5 $\pm$ 8 and 0.5 $\pm$ 6 pmol product/min/pmol enzyme for 0.3uM and 0.1uM enzyme concentrations respectively, as result that aligns with previously conducted research (13).

3.4 Determination of kinetic parameters of CzCdc14

After recognition of CzCdc14 as a phosphatase, the kinetic parameters K_M and V_{max} of the enzyme were determined through a steady-state kinetic analysis. Past studies have given the K_M of ScCdc14 (using pNPP as a substrate) as 10.6 ± 0.9 mM (14). Since ScCdc14 is highly homologous to CzCdc14 (shown in Figure 4), concentrations of pNPP roughly 10 fold above and below the ScCdc14 K_M value

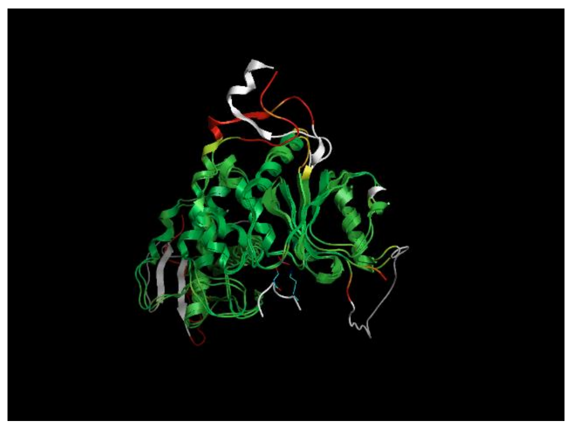

Figure 4. Homology model showing the predicted structure of *C. zeina* Cdc14 based on the X-ray crystal structure of the *S. cerevisiae* Cdc14 (ScCdc14) phosphatase. The translated *C. zeina* gene sequence was input as a query in the MOE software in order to generate a homology model, shown superposed with the template sequence 5XW5.A (the crystal structure of ScCdc14). The model and template are colored by root mean square deviation.

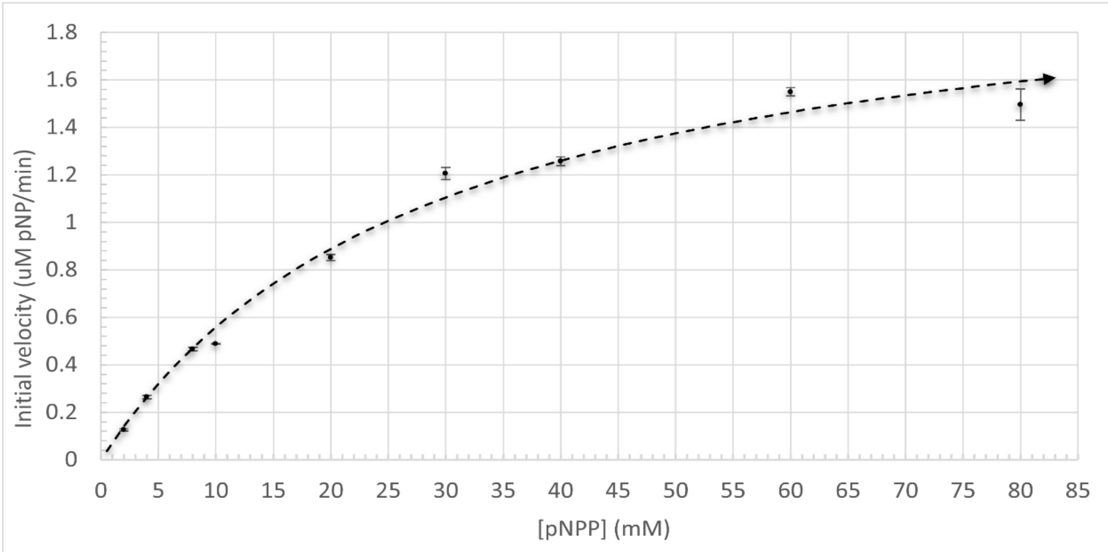

Figure 5. Steady state kinetic analysis of CzCdc14. Three trials of a discontinuous pNPP (*para*-nitrophenyl phosphate) assay were conducted to create a plot of initial velocity versus substrate concentration. Standard deviation was calculated to determine error bars. At a protein concentration of 0.3 µM, CzCdc14 has a K_M value of approximately 28±13 mM and a V_{max} value of approximately 2.17±0.5 µM pNPP/min.

(1 mM to 80 mM) were used in the steady-state assay for *C. zeina.*

The absorbance data was used along with the previously-generated pNP standard curve to calculate product concentration and then initial velocities for CzCdc14 in regards to each substrate concentration. As shown in Figure 5, these initial velocities were plotted against the concentrations of pNP used for the assay in the form of a Michaelis-Menten curve. The steady-

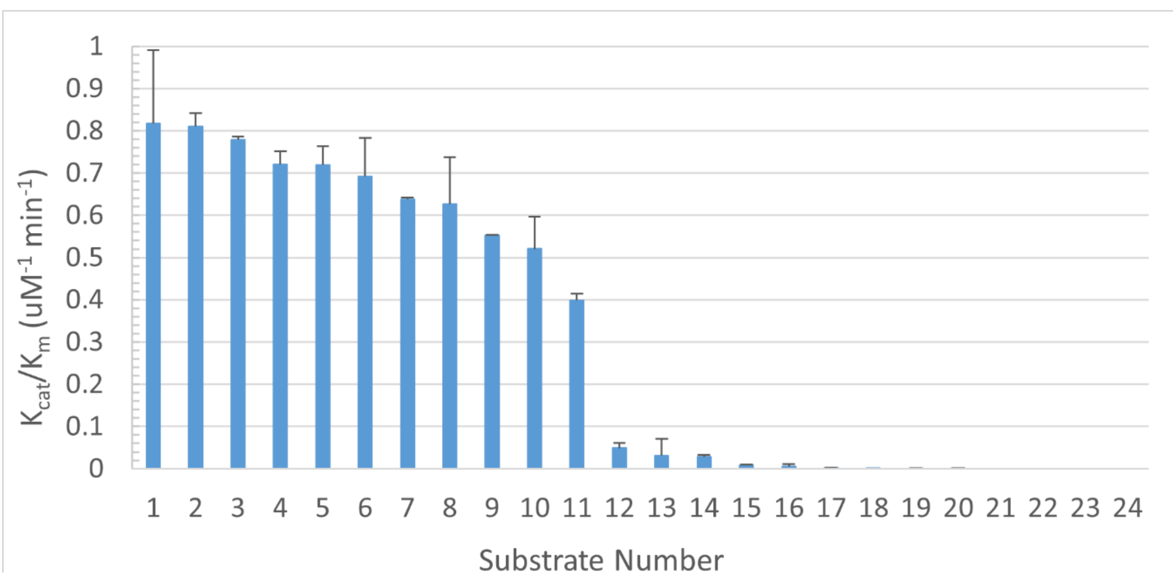

Figure 6. Discontinuous protein activity assay with CzCdc14 and general phosphopeptide substrates. Two trials were conducted where various phosphopeptides acted as substrates for *C. zeina* Cdc14. The degree of dephosphorylation due to enzyme catalysis was characterized quantitatively with Biomol green, a reagent that binds to free phosphate in solution. The data collected was used to determine the specificity constant of each substrate in relation to CzCdc14.

state kinetic analysis was used to determine various kinetic parameters for CzCdc14, including a K_{cat} value of 7$\pm$ 2 μM pNP per minute per uM enzyme and K_M value of roughly 28 $\pm$ 13 mM pNPP.

3.5 Active site identification and substrate specificity analysis

To determine the affinity of CzCdc14 for various substrates, an assay was run that kept enzyme and substrate concentrations constant. A standard curve was generated that had various concentrations of sodium phosphate within a solution of Biomol Green Reagent. Using the generated standard curve shown in Suppl. Figure 3, a specificity assay was run with different phosphopeptide substrates. Previous research suggests that K_M of Cdc14 against general phosphopeptides was 173 ± 21 μM (2) Because a concentration far below this reported K_M was necessary to remain in steady state conditions, 50 μM was used as the substrate concentration in the wells. As shown in Figure 6, final results from the specificity assay indicated that phosphoserine peptides had a higher substrate affinity than phosphothreonine or phosphotyrosine substrates such as 15 or 16. By comparing the general trend of substrate rankings, as well as the ranking of sequences with only single-amino-acid differences, further trends regarding substrate binding could be discerned. For example, it is noticed that in general, the higher-ranking substrates have lysine at the +3 position relative to the phosphorylated residue, a fact that is supported by literature as well (12). By comparing substrates 5 and 8 which differ by one amino acid, it is determined that a +2 isoleucine increases substrate affinity. Many similar conclusions can be drawn, as seen in Figure 7.

Position	Optimal amino acid	Comparision
-2	H	6 and 11
-1	D	5 and 6
phosphopeptide	pS	General Trend
1	P	General Trend
2	I	5 and 8
3	K	General Trend
4	R	3 and 5
5	R	1 and 4
6	G	NA

Figure 7. Predictions for most optimal amino acid by position in substrate sequence. The in vitro data collected on substrate specificity and ranking is utilized to determine the best amino acid for each position in the substrate sequence. The predictions are made based on general trend and specific comparisons between substrates. It should be noted that there is only glycine (G) in position 6, so it is not possible to determine an optimal amino acid at that particular site.

Inhibitor Name	Binding Energy (J)
D7	-6.5078
I1	-6.1812
A1	-6.0375
G7	-5.946
E1	-5.934
G5	-5.616
D3	-5.1099
I9	-4.6991
H7	-4.666
G6	N/A
I2	N/A

Figure 8. Ranking of inhibitors based on binding energy. Binding energy for each inhibitor is calculated by use of Molecular Operating Environment (MOE). Various configurations of inhibitors were generated by MOE, but only the configurations with the greatest binding energy were compiled and recorded. Inhibitors G6 and I2 have no data regarding their binding energy due to their inability to bind to CzCdc14, according to the software.

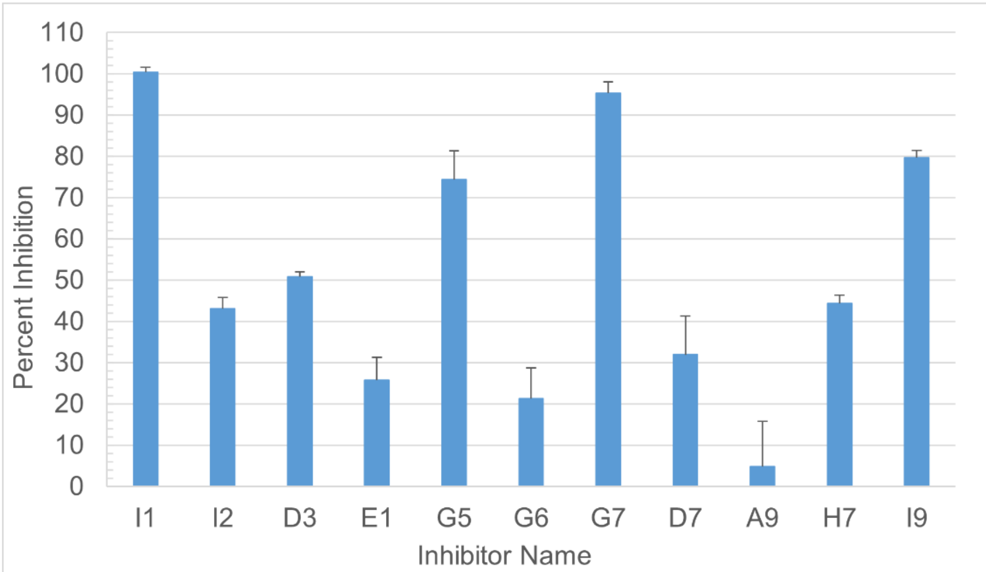

Figure 9. Inhibition of CzCdc14 activity through small molecules of varying concentration. The inhibition is quantified via a discontinuous *para*-Nitrophenylphosphate enzyme assay**.** All inhibitors are at 100 uM concentration except H7 and I9, which are at 1 mM concentration. Three trials for each inhibitor were run for 25 minutes at 0.1 μM enzyme and 25 mM pNPP. The average and standard deviation of the three trials for each inhibitor are calculated and displayed as bars and error bars respectively. The percent inhibition values of the three most effective inhibitors are 100 ± 1 (I1), 95 ± 3 (G7), and 80. ± 2 (I9).

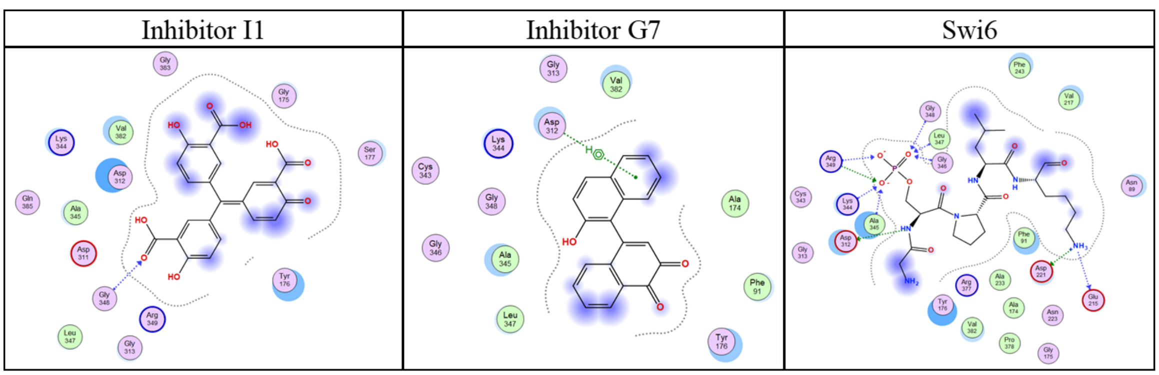

Figure 10. Ligand interaction maps for the binding of Inhibitor I1, I7 as well as the natural substrate Swi6. The Molecular Operating Environment (MOE) was used to generate the interaction maps containing amino acids found in the active site. Amino acids which interact with the substrate/inhibitor are represented by dotted lines. Blue lines represent backbone interactions, green lines represent side chain interactions.

3.6 Determination of inhibitor candidates

Various inhibitors identified in high-throughput screening were tested to identify characteristics that could be used to create a potential fungicide for CzCdc14 (2). Trials of 10 different inhibitors were run in triplicates that held the concentrations of the CzCdc14, pNPP substrate, and different inhibitors constant. Average absorbance values across the three trials for each inhibitor were measured and used to calculate their percent inhibition. In addition, standard deviation for each set of three trials were calculated and plotted as shown in Figure 9.

After ranking the collected data in Figure 9, inhibitors I1, G7, I9, and G5 were determined to be the most effective against CzCdc14. However, due to the higher concentration of I9 that was present in the wells during inhibition screening, it was removed as a potential candidate for CzCdc14.

To further determine the best inhibitors for CzCdc14, the inhibitors were ranked based on binding energy. Figure 8 ranks inhibitors based on their binding energy to the enzyme that was predicted by MOE. However, data received from MOE and the data measured in the lab had poor correspondence.

In addition to binding energy, interactions between the inhibitor and the CzCdc14 active site residues were considered in the rank determination. Ligand interaction maps were generated in order to gauge which inhibitor molecules bound most optimally to the enzyme. Inhibitors whose ligand interaction maps showed most/all of the seven identified catalytic CzCdc14 residues (Cys 343 in particular) were ranked highest.

Figure 10 shows the interactions of inhibitors I1 and G7 with the catalytic residues of CzCdc14 (Asp 312, Cys 343, Lys 344, Ala 345, Leu 347, Gly 348, Arg 349, as seen in Suppl. Figure 5) in comparison to the interactions of these residues with the phosphopeptide substrate Swi6. I1 is shown to interact with all catalytic residues except Cys 343, and G7 interacts with all except Arg 349. Considering binding energies, interactions with active site residues, and lab data, inhibitors I1 and G7 were selected for IC_{50} value determination.

To calculate IC_{50} for inhibitors I1 and G7, a sigmoidal curve was generated wherein the inflection point of the graph approximates IC_{50} for each inhibitor. To create the sigmoidal curve, trials were run at various concentrations of the specified inhibitors (while enzyme concentration and substrate concentration were held constant).

The calculated IC_{50} was 2.5 ± 0.3 μM and 18 ± 1 μM for Inhibitors I1 and G7 respectively. Evidently, I1 is a viable inhibitor for CzCdc14, thus, a promising fungicide candidate for GLS.

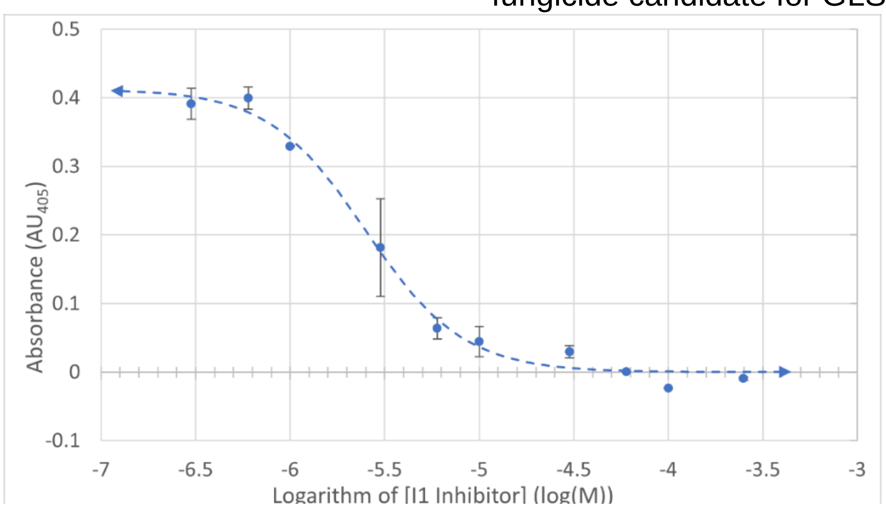

Figure 11. Inhibition of CzCdc14 activity by differing concentrations of aurintricarboxylic acid (inhibitor I1). The inhibition of CzCdc14 is quantified via a discontinuous *para*-Nitrophenyl phosphate enzyme assay. Inhibitor concentrations ranging from 300nM to 250uM are used in the assay, along with 0.1uM enzyme and 25mM pNPP. The absorbance of each reaction trial after 20 minutes of catalytic activity is measured, and the average of the trials are plotted against the logarithm of inhibitor concentration to determine IC_{50}. Error bars represent the standard deviation of the trials.

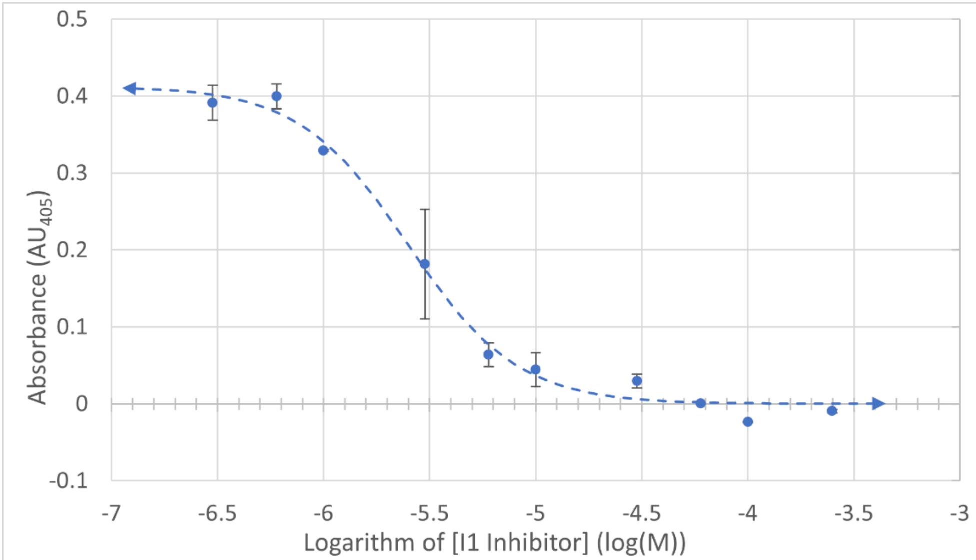

Figure 12. Inhibition of CzCdc14 activity by differing concentrations of 2'-hydroxy-[1,1'-binaphthalene]-3,4-dione (inhibitor G7). The inhibition of CzCdc14 is quantified via a discontinuous *para*-Nitrophenyl phosphate enzyme assay. Inhibitor concentrations ranging from 300nM to 250uM are used in the assay, along with 0.1uM enzyme and 25mM pNPP. The absorbance of each reaction trial after 20 minutes of catalytic activity is measured, and the average of the trials are plotted against the logarithm of inhibitor concentration to determine the IC_{50}. Error bars represent the standard deviation of the trials.

DISCUSSION:

We showed that CzCdc14 is highly similar to other fungal Cdc14 homologs with respect to kinetic characteristics. One of our more significant conclusions in this area is that the K_m of CzCdc14 with pNPP as a substrate is 28 ± 13 mM, which is within the same order of magnitude as the the reported K_m for ScCdc14 with the same substrate, 10.6 ± 0.9 mM (14). This supports the idea of Cdc14 active site conservation in *C. zeina* in relation to similar species; if Cdc14 affinity and catalytic rate are similar between *C. zeina* and species like *S. cerevisiae* for the same substrate, it follows that the Cdc14 catalytic residues are well-conserved between such species.

We also found that the requirements of CzCdc14 substrate recognition adhere relatively well to the general set of substrate recognition features that describe fungal Cdc14 phosphatases at large. For example, the phosphopeptide substrates that bound to CzCdc14 most successfully had a Ser as their phosphorylated residue, a Pro at the +1 position relative to this phosphoserine, and a basic residue (specifically Lys) at the +3 position, which are all features cited as important to Cdc14 substrate recognition in species like *S. cerevisiae* (2). Further, a multiple sequence alignment generated through the Clustal Omega software revealed that the active site residues for the species *Alternaria alternata, Penicillium digitatum, Puccinia coronata, Rhynchosporium commune, Ustilago hordei* were perfect matches to each other and to those of *C. zeina* (see Supplemental Figure 5), again showing the high degree of Cdc14 catalytic conservation within the fungal kingdom.

Still, there remain inconsistencies regarding some substrate binding specifications between CzCdc14 and those of other Cdc14 homologs. For example, an ideal empirical result would have been that *A. alternata, P. digitatum, P. coronata, R. commune, U. hordei*, and *C. zeina* would have had the same best and worst inhibitor molecules in the above-described inhibition assay. However, I1 (the most effective inhibitor of CzCdc14) was not the best inhibitor for all the aforementioned species, nor was A9 (the least effective inhibitor of CzCdc14) the worst for all species. A possible explanation for this result relates to evolutionary divergences; though the active site residues themselves are entirely conserved between fungal species, the amino acids immediately adjacent to these catalytic residues are not so highly conserved. Differences in the properties of these adjacent amino acids may be the cause of discrepancies in which molecules bind best to Cdc14 from different fungal species.

Inconsistencies were also observed between in silico predictions and experimental results regarding the effectiveness of the small-molecule inhibitors we tested. For instance, the inhibitor predicted to be most successful in MOE (where rankings were based primarily on binding energy) was D7, but in the physical assay procedure, this molecule was not within the top-ranking inhibitors. The explanation for such differences, however, can be found in the inability of the MOE software to take into account covalent interactions between ligands and enzymes. Because all small molecules used in the inhibition assay employed covalent mechanisms (save H7), the generated computational models could not accurately reflect the actual interactions between our inhibitor candidates and CzCdc14. In addition, the presence of highly electronegative atoms is more heavily weighted in MOE-based ranking than this feature is in vitro. Consequently, inhibitor molecules rich in such atoms (such as D7) were predicted to be more effective than they proved to be assay-wise.

Taking this reasoning into account, we used our empirical inhibition results to conduct further computational research into optimal inhibitor properties for CzCdc14. The most effective inhibitor seen experimentally (I1) was modeled and modified in MOE: two SO2 functional groups and a six-carbon ring were added, an oxygen atom was replaced with an imidazole ring, and a hydrogen atom was replaced with sulfur. These changes resulted in a 29.2% increase in binding affinity score, suggesting that I1 is a viable CzCdc14 inhibitor candidate for chemical alteration and subsequent real-world use (Suppl. Figure 6).

These results and computational predictions justify further experimentation–specifically chemical modification–on our top-ranking inhibitor molecules based on their in vitro performance. Again, the strong similarities between Cdc14 in *C. zeina* and related fungal species may allow for the use of a CzCdc14 inhibiting molecule with other fungal pathogens; a CzCdc14-targeting fungicide can thus have broad functionality and important applications in the agricultural industry.

REFERENCES:

1. Swart, V., Crampton, B. G., Ridenour, J. B., Bluhm, B. H., Olivier, N. A., Meyer, J. J. M., & Berger, D. K. (2017). Complementation of *CTB7* in the Maize Pathogen *Cercospora zeina* Overcomes the Lack of In Vitro Cercosporin Production. *Molecular Plant-Microbe Interactions®*, *30*(9), 710–724. https://doi.org/10.1094/mpmi-03-17-0054-r
2. DeMarco, A. G., Milholland, K. L., Pendleton, A. L., Whitney, J. J., Zhu, P., Wesenberg, D. T., Nambiar, M., Pepe, A., Paula, S., Chmielewski, J., Wisecaver, J. H., Tao, W. A., & Hall, M. C. (2020). Conservation of Cdc14 phosphatase specificity in plant fungal pathogens: implications for antifungal development. *Scientific Reports*, *10*(1). https://doi.org/10.1038/s41598-020-68921-3
3. Ward, J. M. J., Stromberg, E. L., Nowell, D. C., & Nutter, F. W. (1999). Gray leaf Spot: A Disease of Global Importance in Maize Production. *Plant Disease*, *83*(10), 884–895. https://doi.org/10.1094/pdis.1999.83.10.884
4. Nsibo, D. L., Barnes, I., Omondi, D. O., Dida, M. M., & Berger, D. K. (2021). Population genetic structure and migration patterns of the maize pathogenic fungus, Cercospora zeina in East and Southern Africa. *Fungal Genetics and Biology*, *149*, 103527. https://doi.org/10.1016/j.fgb.2021.103527
5. Benson, J. M., Poland, J. A., Benson, B. M., Stromberg, E. L., & Nelson, R. J. (2015). Resistance to Gray Leaf Spot of Maize: Genetic Architecture and Mechanisms Elucidated through Nested Association Mapping and Near-Isogenic Line Analysis. *PLOS Genetics*, *11*(3), e1005045. https://doi.org/10.1371/journal.pgen.1005045
6. Queralt, E., & Uhlmann, F. (2008). Cdk-counteracting phosphatases unlock mitotic exit. *Current Opinion in Cell Biology*, *20*(6), 661–668.

https://doi.org/10.1016/j.ceb.2008.09.003

7. He, W., Zhu, Y., Leng, Y., Yang, L., Zhang, B., Yang, J., Zhang, X., Lan, H., Tang, H., Chen, J., Gao, S., Tan, J., Kang, J., Deng, L., Li, Y., He, Y., Rong, T., & Cao, M. (2021). Transcriptomic Analysis Reveals Candidate Genes Responding Maize Gray Leaf Spot Caused by Cercospora zeina. *Plants*, *10*(11), 2257. https://doi.org/10.3390/plants10112257
8. Nyanapah, J. O., Ayiecho, P. O., Nyabundi, J. O., Otieno, W., & Ojiambo, P. S. (2020). Field Characterization of Partial Resistance to Gray Leaf Spot in Elite Maize Germplasm. *Phytopathology®*, *110*(10), 1668–1679. https://doi.org/10.1094/phyto-12-19-0446-r
9. Muller, M. F., Barnes, I., Kunene, N. T., Crampton, B. G., Bluhm, B. H., Phillips, S. M., Olivier, N. A., & Berger, D. K. (2016). *Cercospora zeina* from Maize in South Africa Exhibits High Genetic Diversity and Lack of Regional Population Differentiation. *Phytopathology®*, *106*(10), 1194–1205. https://doi.org/10.1094/phyto-02-16-0084-fi
10. Kobayashi, J., & Matsuura, Y. (2017). Structure and dimerization of the catalytic domain of the protein phosphatase Cdc14p, a key regulator of mitotic exit in *Saccharomyces cerevisiae*. *Protein Science*, *26*(10), 2105–2112. https://doi.org/10.1002/pro.3244
11. Visintin, R., Craig, K., Hwang, E. S., Prinz, S., Tyers, M., & Amon, A. (1998). The Phosphatase Cdc14 Triggers Mitotic Exit by Reversal of Cdk-Dependent Phosphorylation. *Molecular Cell*, *2*(6), 709–718. https://doi.org/10.1016/s1097-2765(00)80286-5
12. Bremmer, S. C., Hall, H., Martinez, J. S., Eissler, C. L., Hinrichsen, T. H., Rossie, S., Parker, L. L., Hall, M. C., & Charbonneau, H. (2012). Cdc14 Phosphatases Preferentially

Dephosphorylate a Subset of Cyclin-dependent kinase (Cdk) Sites Containing Phosphoserine. *Journal of Biological Chemistry*, *287*(3), 1662–1669. https://doi.org/10.1074/jbc.m111.281105

13. Traverso, E. E., Baskerville, C., Liu, Y., Shou, W., James, P., Deshaies, R. J., & Charbonneau, H. (2001). Characterization of the Net1 Cell Cycle-dependent Regulator of the Cdc14 Phosphatase from Budding Yeast. Journal of Biological Chemistry, 276(24), 21924–21931. https://doi.org/10.1074/jbc.m011689200

14. Gray, C. H. (2003). The structure of the cell cycle protein Cdc14 reveals a proline-directed protein phosphatase. *The EMBO Journal*, *22*(14), 3524–3535. https://doi.org/10.1093/emboj/cdg348

15. Wang, W. Q., Bembenek, J., Gee, K. R., Yu, H., Charbonneau, H., & Zhang, Z. Y. (2004). Kinetic and Mechanistic Studies of a Cell Cycle Protein Phosphatase Cdc14. Journal of Biological Chemistry, 279(29), 30459–30468. https://doi.org/10.1074/jbc.m402217200

SUPPLEMENTAL DATA:

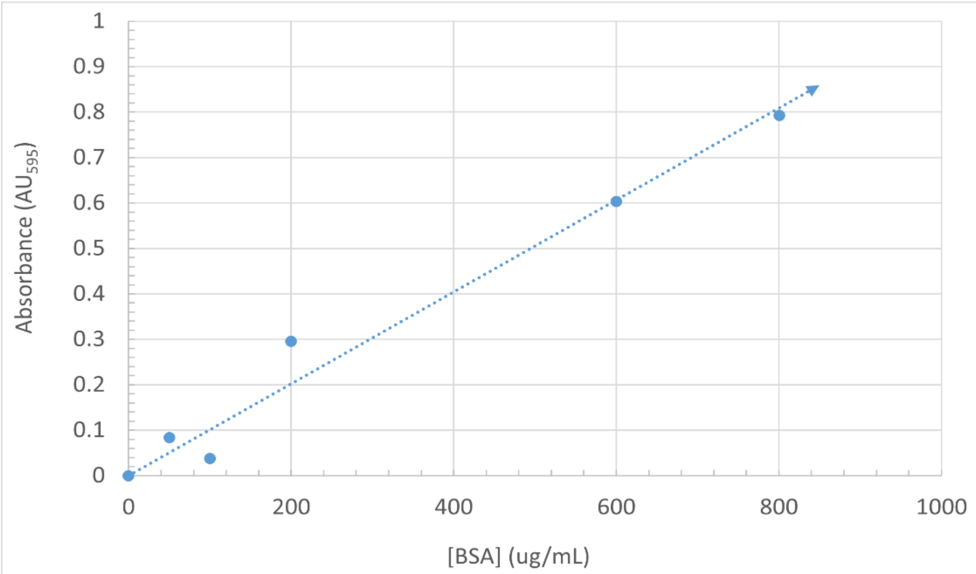

Suppl. Figure 1. Absorbance of differing concentrations of bovine serum albumin (BSA). Differing concentrations of BSA ranging from 0 to 800 ug/mL are combined with Bradford reagent dye and scanned by a spectrophotometer at 595 nm. The collected data is used to create a standard curve. The line of best fit for the standard curve is characterized by the equation: AU = 0.001 [BSA]. The R^2 value is 0.987.

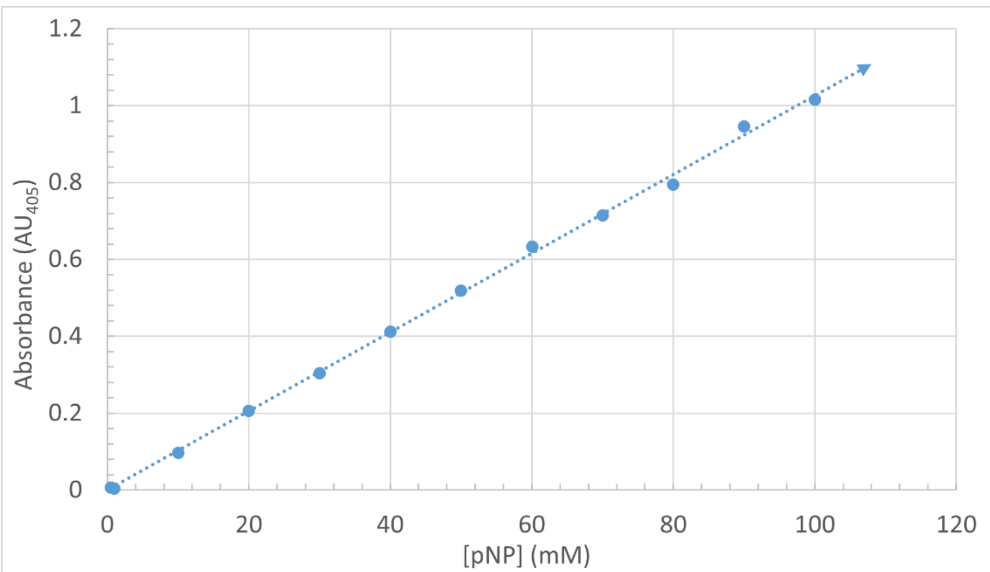

Suppl. Figure 2. Absorbance of differing concentrations of *para*-Nitrophenyl (pNP). Differing concentrations of pNP are scanned by a plate reader at a wavelength of 405 nm, and a standard curve is created from the collected data. The line of best fit for the standard curve is characterized by the equation: AU = 0.0103 [pNP]. The R^2 value is 0.9996.

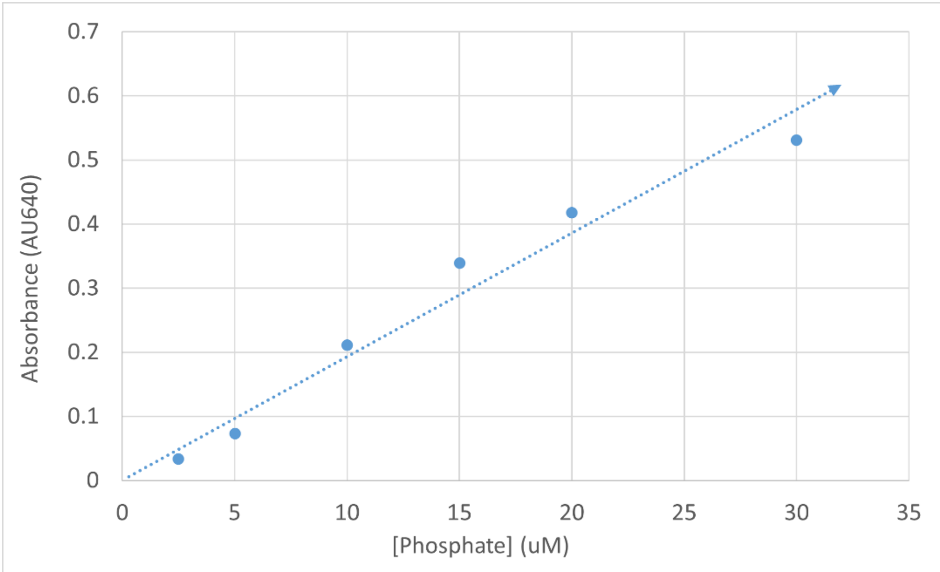

Suppl. Figure 3. Absorbance of differing concentrations of phosphate ions. Differing concentrations of phosphate ranging from 2.5 uM to 30uM are combined with Biomol Green reagent dye and scanned by a plate reader at 595 nm wavelength light. The collected data is used to create a standard curve. The line of best fit for the standard curve is characterized by the equation: AU = 0.0193 [Phosphate]. The R^2 value is 0.989

Substrate Number	Phosphopeptide sequence	Substrate Number	Phosphopeptide sequence
1	HT{pS}PIKSRG	13	HT{pS}PIAKIG
2	HT{pS}PKKRIG	14	HT{pS}PIRSIG
3	HT{pS}PIKRIG	15	HT{pY}PIKSIG
4	HT{pS}PIKSKG	16	HT{pT}PIKSIG
5	HD{pS}PIKSIG	17	HT{pS}PIASKG
6	HT{pS}PIKSIG	18	HT{pS}GIKSIG
7	HT{pS}PIKKIG	19	HT{pS}GIKRIG
8	HT{pS}PKKSIG	20	HT{pS}PKASIG
9	HT{pS}PEKSIG	21	HT{pS}AIKSIG
10	HT{pS}PRKSIG	22	HT{pS}GIASIG
11	RT{pS}PIKSIG	23	HT{pS}PIASIG
12	HT{pS}PPKSIG	24	HT{pS}PILSIG

Suppl Figure 4. Phosphopeptide sequences for each substrate. The phosphopeptides were numbered based on rankings determined by in-vitro experimentation

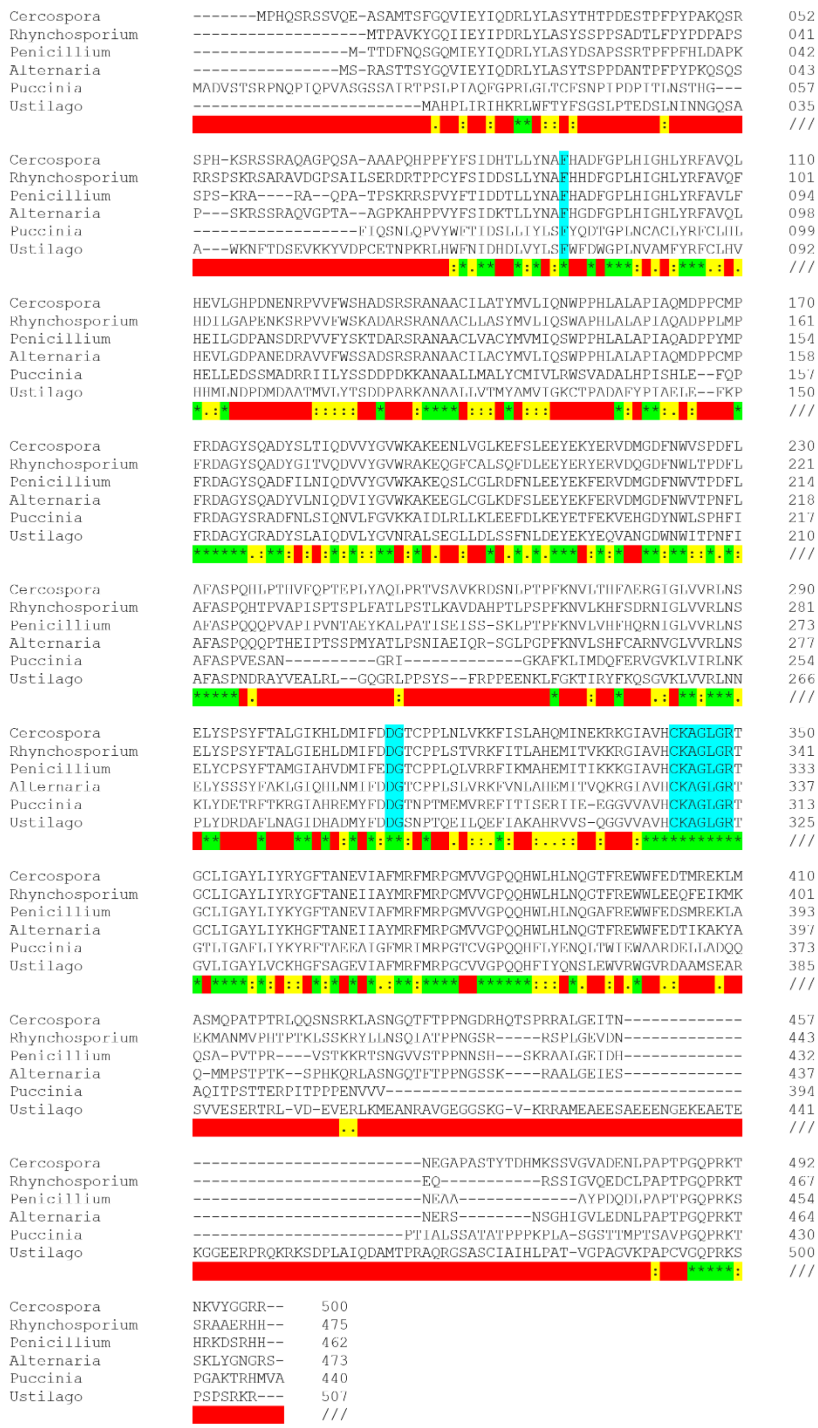

Suppl. Figure 5. In-silico alignment of Cdc14 phosphatase protein sequence for numerous pathogenic fungal species. The multiple sequence alignment tool Clustal Omega is used to align and compare the amino acid sequences of Cdc14 phosphatase from different fungi. Fully preserved sequences are represented in green and highly conserved sequences (4 or more of the 6 species contain the same amino acid) are colored yellow. The binding pocket sequences of Cdc14 phosphatase are identified by the Molecular Operating Environment, and highlighted blue. Clustal Omega identified that all binding pocket amino acids are completely conserved between the 6 fungal species.

Initial Interaction Map	Initial 3D Structure
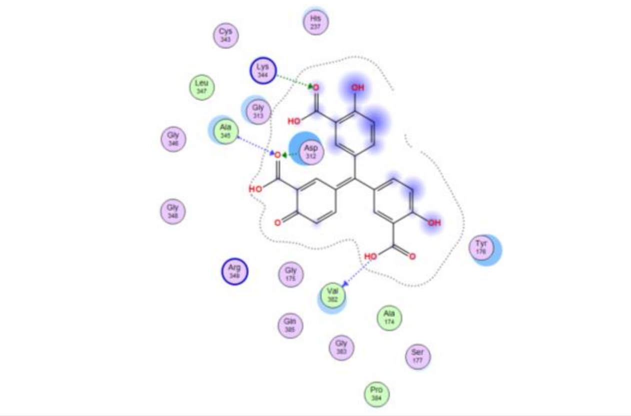	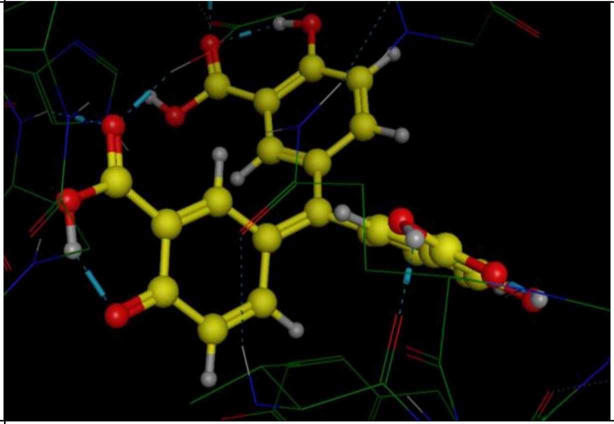
Final Interaction Map	Final 3D Structure
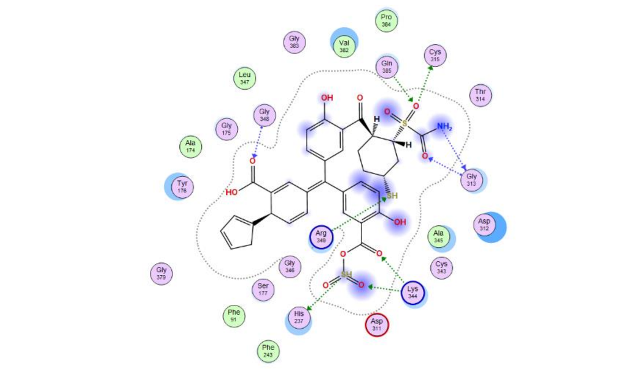	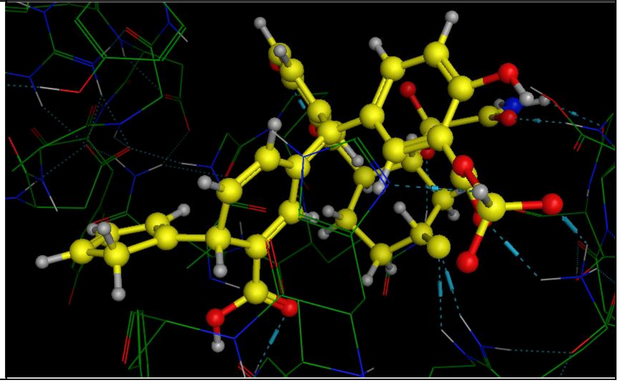

Suppl. Figure 6. Optimization of I1 inhibitor via MOE software. New functional groups were introduced to the I1 inhibitor, and the binding affinity for the new inhibitor was calculated. After 6 iterations of this process, the affinity of the inhibitor increased by 29.2%.

Abbreviated Name	Compound Name	Structure
A9	2-amino-4-(2,3-dichlorophenyl)-7-hydroxy-4H-chromene-3-carbonitrile	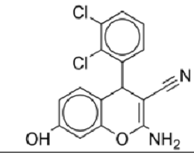
D3	3-(5-(2-bromophenyl)furan-2-yl)acrylic acid	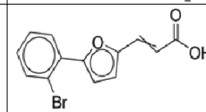
D7	3-((2,4,6-trioxotetrahydropyrimidin-5(2 H)-ylidene)methyl)phenyl 3-fluorobenzoate	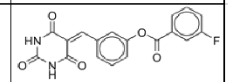
E1	5-(5-chloro-2-hydroxy-3-nitrobenzylidene)-1,3-dimethylpyrimidine-2,4,6(1H,3H,5H)-trione	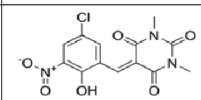
G5	5-(4-isopropylbenzylidene)pyrimidine-2,4,6(1H,3H,5H)-trione	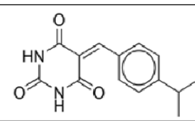
G6	sodium 3,4-dioxo-3,4-dihydronaphthalene-1-sulfonate	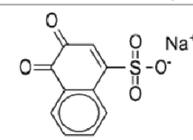
G7	2'-hydroxy-[1,1'-binaphthalene]-3,4-dione	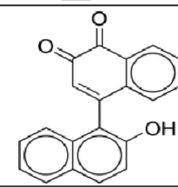
H7	7-methylimidazo[1,2-a]pyridine-2-carboxylic acid	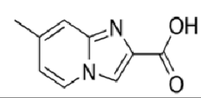
I1	aurintricarboxylic acid	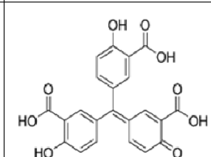
I2	benserazide hydrochloride	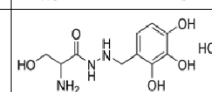
I9	6-bromo-7-hydroxy-2-(methylamino)-thiazolo[4,5-b]pyridin-5(4H)-one	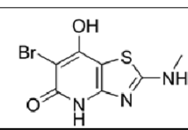

Suppl. Figure 7. Name and structure for inspected inhibitors. The IUPAC names and corresponding chemical structures are listed according to inhibitor code names.